Supplementary file, Zhao et al., (2012)

1. **Figure DR1.** Summary of geoelectric strike directions.
2. **Figure DR2a,b,c.** Apparent Resistivity and phase curves for each profile (L1, L2 and L4), showing the fit of the inversion model to the measured MT data.
3. **Figure DR3a,b,c.** Pseudosections for each profile（L1, L2 and L4）, also showing the fit of the predicted responses to the measured MT data.
4. **Figure DR4.** L-curves for profiles L1, L2 and L4.
5. **Table DR1.** Parameters for profiles L1, L2 and L4.
6. **Table DR2.** Parameters used in the inversion and r.m.s misfit for each profiles.
7. **Table DR3a,b,c.** Static shift correction factors for L1,L2 and L4
8. **Item 8.** Supplementary Discussion: Data collection, details of inversion and interpretation.

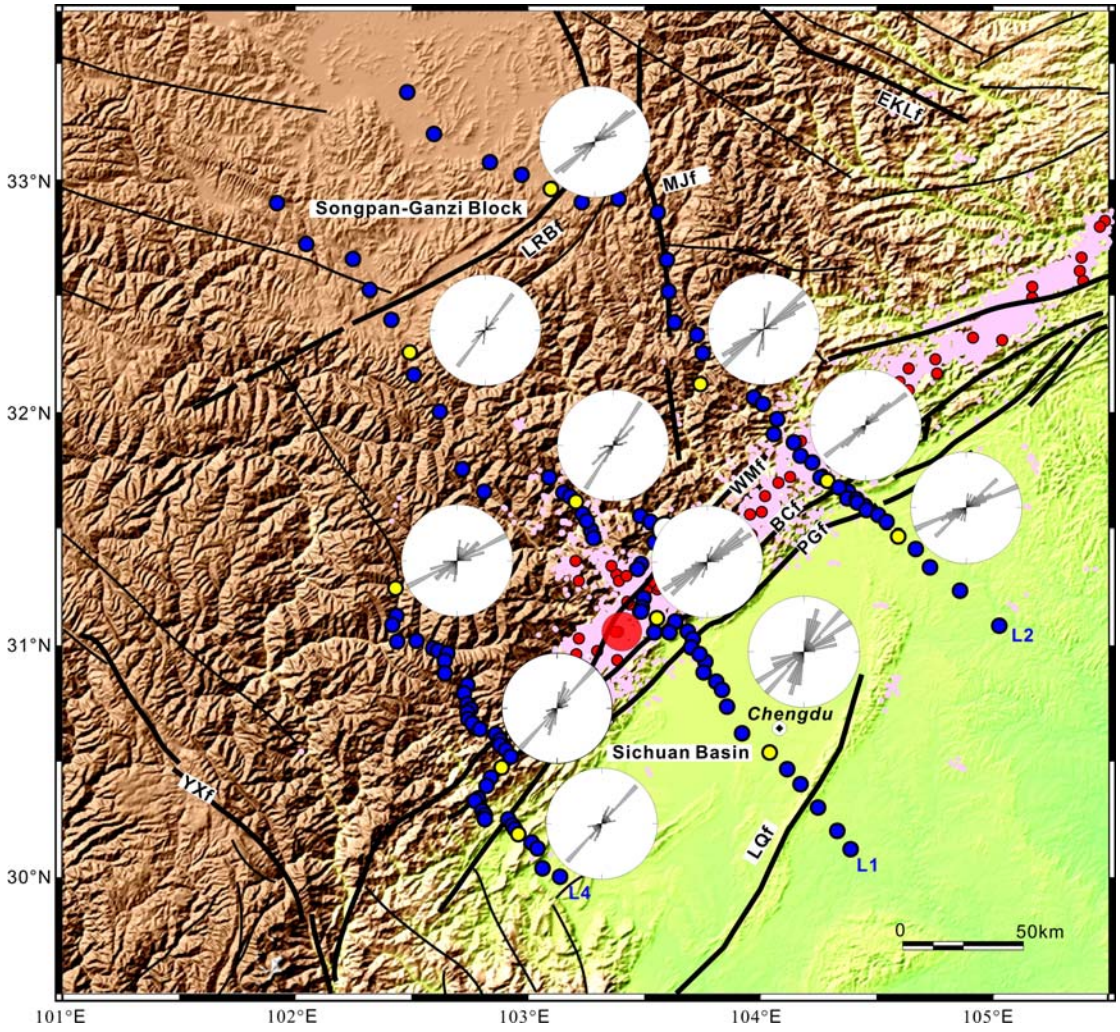

Figure DR1. Map showing MT profiles (L2, L1, and L4) sites (blue circles), main Wenchuan earthquake (large red circle, May 12, 2008, at depth of 14-19 km) and aftershocks (small red circles aftershocks with M≥5 and pink dots show aftershocks 2≤M<5) epicenters (Zhu et al., 2008, in main text) of the Wenchuan earthquake in Longmenshan range. The coseismic rupture along the main fault (BCf) was about 240 – 300 km in length, with maximum vertical and horizontal displacements of 6.5 m and 4.9 m respectively (Xu et al., 2009, in main text). The rupture along the east fault (PGf) was 90 km long (Xu et al., 2009, in main text). The coseismic ruptures propagated towards the northeast from the hypocenter area along the fault zone (Zhang Y et al., 2009, in main text). The rose diagrams show the geoelectric strike

direction at the stations plotted in yellow. The geoelectric strike direction is in a NE-SW direction, in good agreement with the geologic strike of the Longmenshan. YXf = Yushu-Xianshuihe fault, EKLf = East Kunlun fault, LRBf=Longriba fault, MJf=Minjiang fault, LQf=Longquan fault, WMf = Wenchuan-Maoxian fault, BCf = Beichuan fault (BCf) and PGf = Penguan fault (PGf).

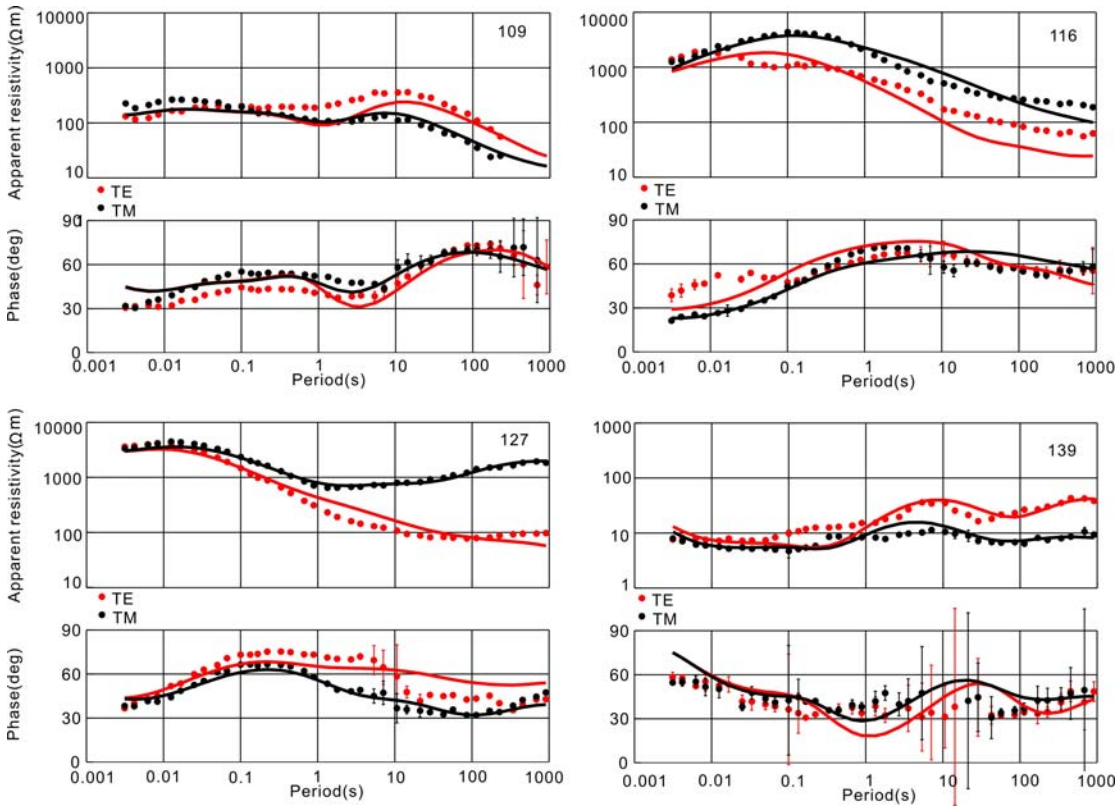

Figure DR2a. Typical apparent resistivity and phase curves at MT sites 109, 116, 127 and 139 on profile L1. These quantities are the measured data in an MT survey and described for non-experts by Simpson and Bahr (2005). The circles show the measured MT data, and the line shows the response of the inversion models in Figure 2. TE = transverse electric mode with electric current flowing parallel to the geoelectric strike direction (N45°E), and TM = transverse magnetic mode with electric current flowing perpendicular (N135°E) to the geoelectric strike direction. The curves indicate the resistivity variation along the profile which is consistent with the pseudosection in Fig.DR3a.

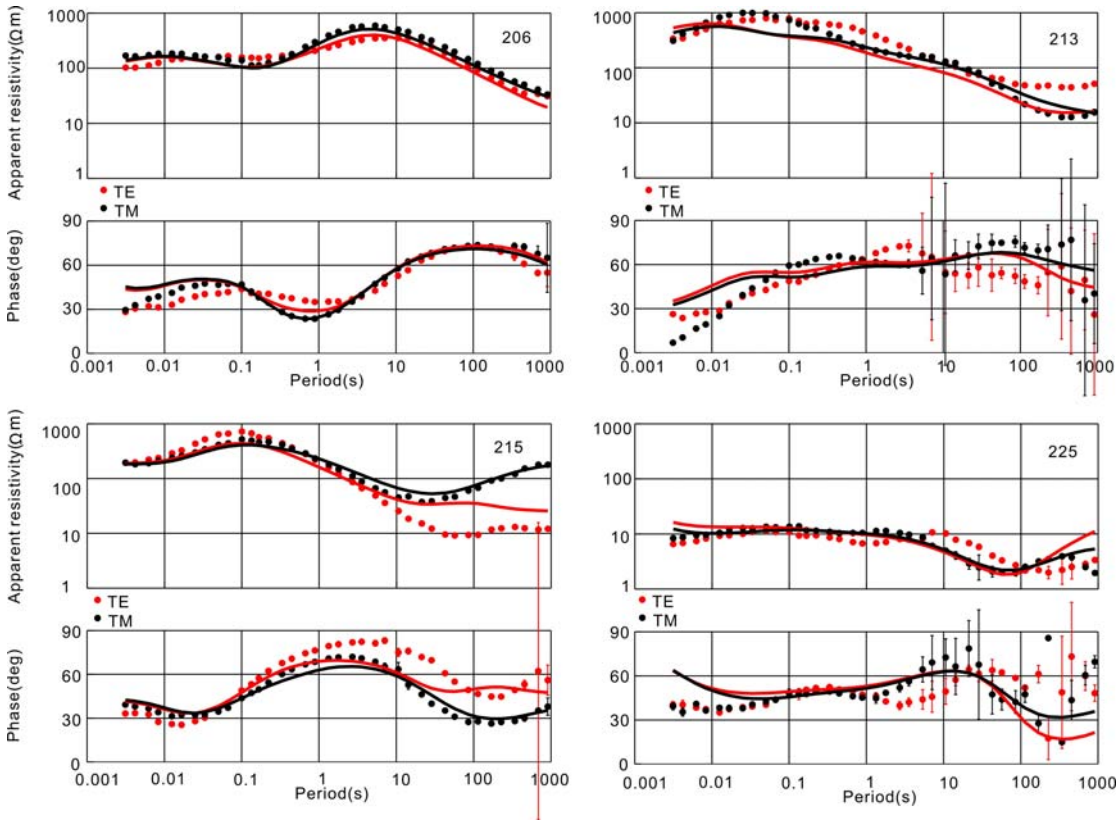

Figure DR2b. Apparent resistivity and phase curves for sites 206, 213, 215 and 225 on profile 2. The symbols have the same meaning as in Fig. DR2a. The curves show the resistivity variation along the profile which is consistent with the pseudosection in Fig.DR3b.

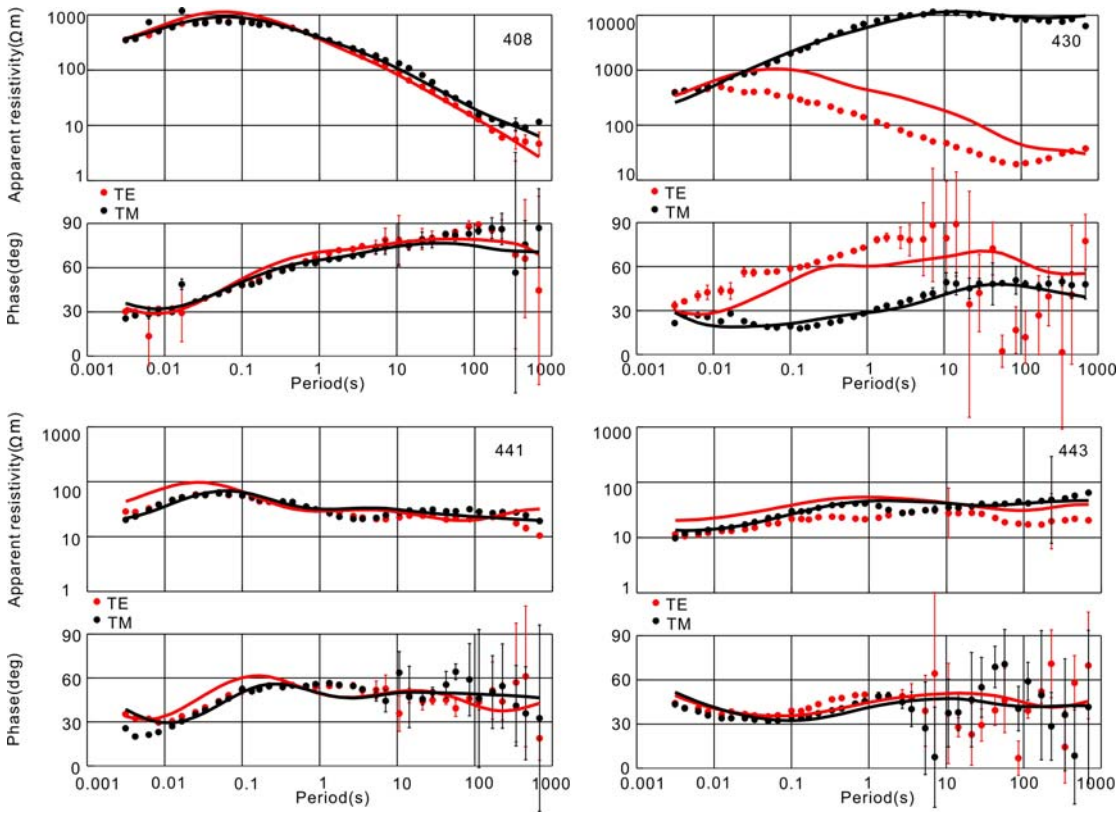

47

48 **Figure DR2c.** Apparent resistivity and phase curves for sites 408,430,441 and 443 on

49 L4. Labeling is the same that in Fig.DR2a. The curves indicate the resistivity variation

50 along the profile which is consistent with the pseudosection in Fig.DR3c.

51

52

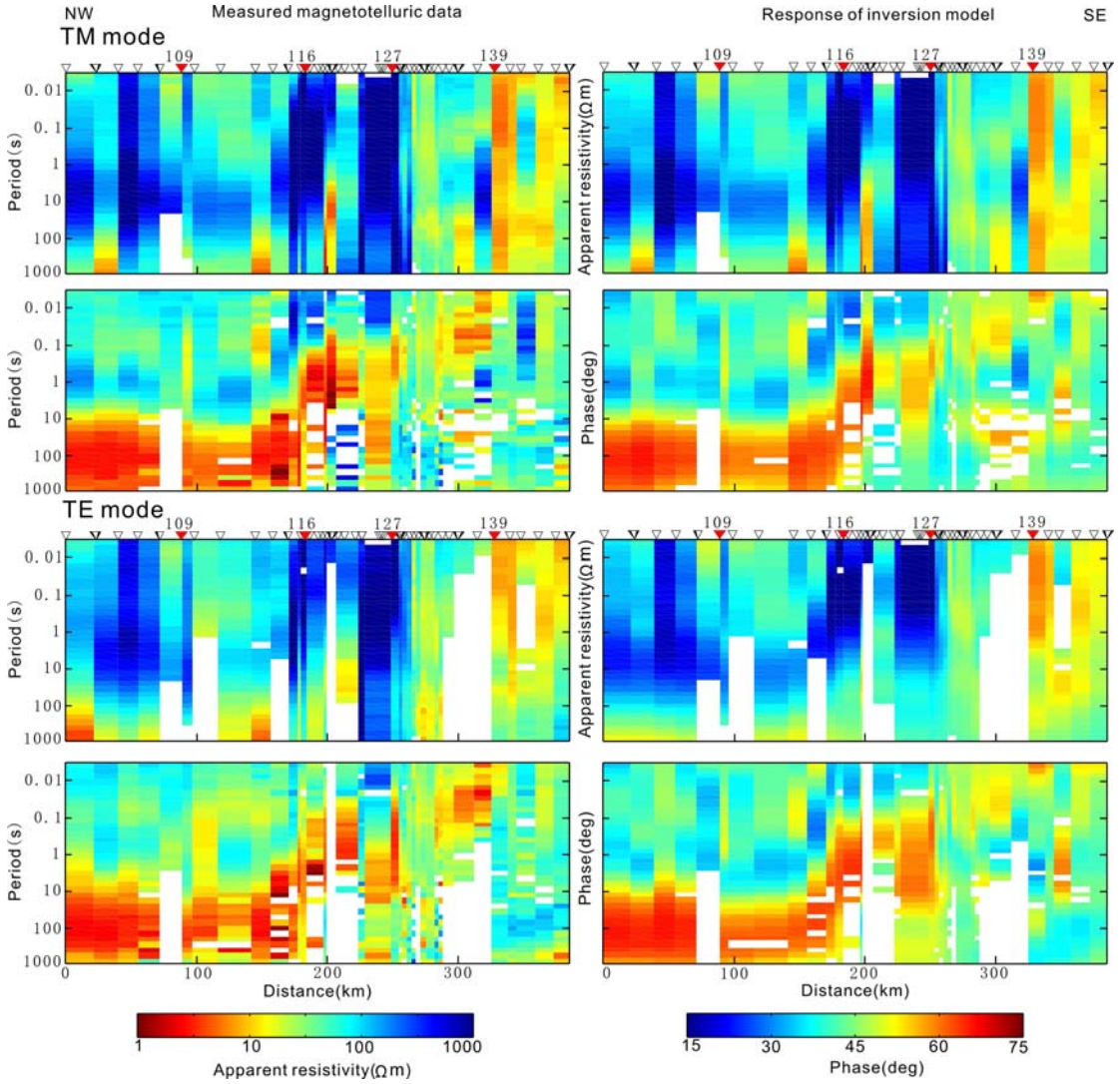

Figure DR3a. The left column shows pseudosections of the measured MT apparent resistivity and phase on profile L1. The right column shows the corresponding pseudosections of the response of the inversion model for profile L1. Note the high phase values in both the TM (top four panels) and TE (bottom four panels) modes in the period band T = 10-1000 s at a distance of 0-230 km, which are caused by the high conductive layer (HCL) beneath the Songpan-Ganzi block. The low phase values in both the TM and TE modes in the period band T = 0.01-1.0 s at distances of 230-310 km are caused by the high resistivity zone (HRB) in the inversion model in Figure 2 at the same offsets. The locations of the MT stations from Figure S2a are shown as red triangles, labeled with the station number. Note the good agreement between the measured MT data and the response of the inversion model. White regions denote data that was excluded because of noise.

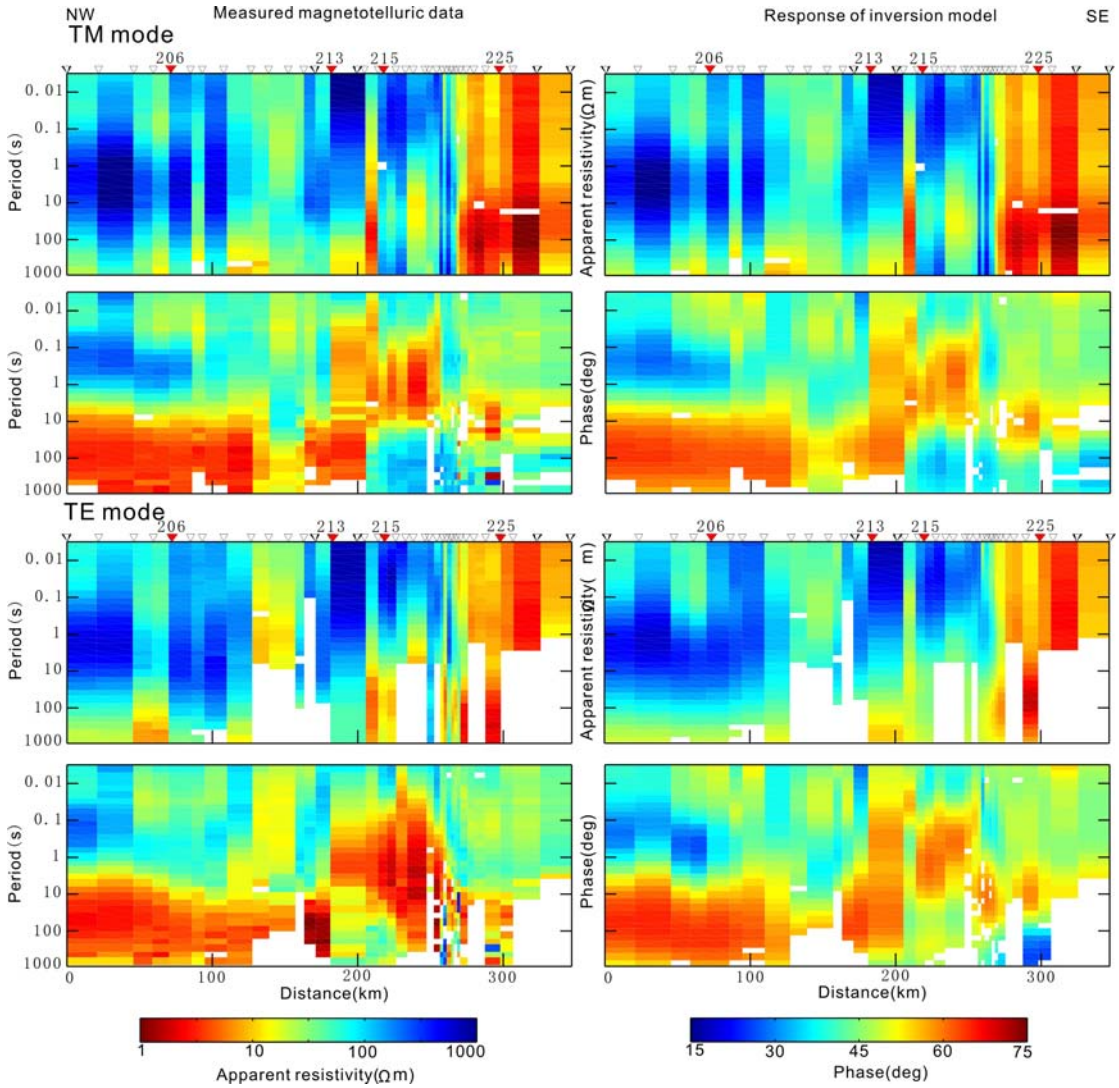

Figure DR3b. The left column shows pseudo-sections of the measured MT apparent resistivity and phase data for profile L2. The right column shows corresponding pseudo-sections of the response of inversion model on profile L2. Note the high phase values in both the TM (top four panels) and TE (bottom four panels) modes in the period band T = 10-1000 s band at distances of 0-180 km, which are caused by the high conductive layer (HCL) beneath the Songpan-Ganzi block. The low phase values in both the TM and TE modes in the period band T = 0.01-1.0 s at distance of 180-260 km are caused by the high resistivity zone (HRB) in the inversion model in Figure 2 at the same offsets. The locations of the stations from Figure DR2b are shown as red triangles, labeled with the station number.

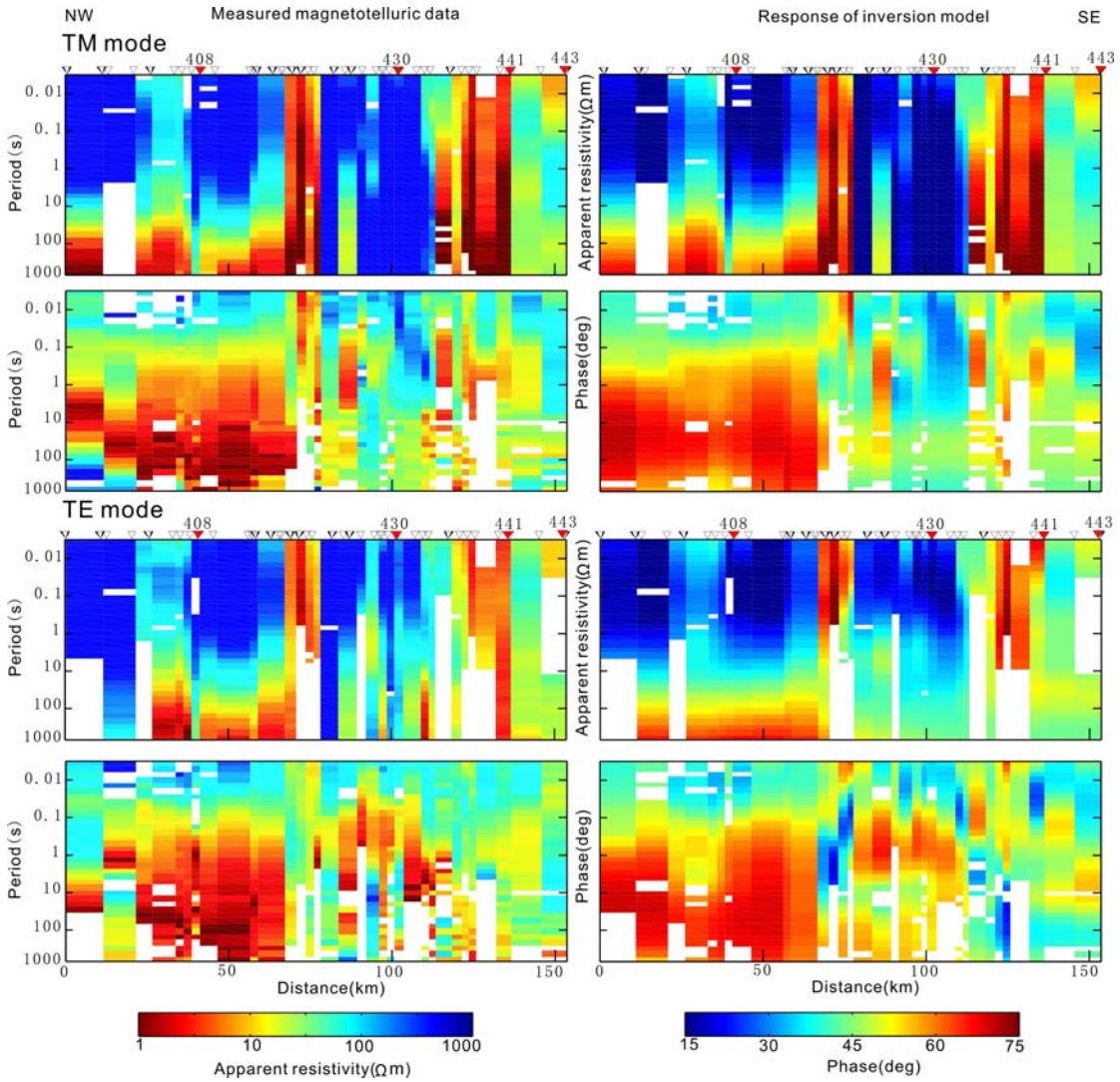

Figure DR3c. The left column shows pseudo-sections of the measured MT apparent resistivity and phase on profile L4. The right column shows corresponding pseudosections of the response of the inversion model for profile L4. Note the high phase values in both the TM (top four panels) and TE (bottom four panels) modes in the period band T = 0.1-100 s band at distances of 0-75 km, which are caused by the high conductive layer (HCL) beneath the Songpan-Ganzi block. The low phase values in both the TM and TE modes in the period band T = 0.01-1.0 s at distances of 75-120 km are caused by the high resistivity zone (HRB) in the inversion model in Figure 2 at the same offsets. The locations of stations from Figure DR2c are shown as red triangles, labeled with the station number.

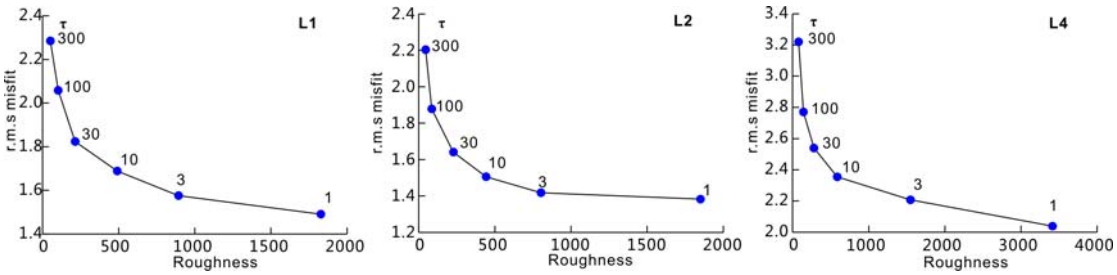

Figure DR4. L-curves for models of the data from profiles L1, L2 and L4 show the trade-off between model roughness (complexity) and fitting the measured MT data. Tau=10 is considered to be the corner of the L-curve in each case, and is used for the final model of each of three profiles respectively because it is the best choice for modeling of three profiles. The inverted models show that the r.m.s misfit increased and the model became smooth when τ was increasing. Conversely, the r.m.s. misfit decreased and the model became roughner.

Table DR1. Parameters for profiles L2, L1 and L4

Profile	Length (km)	Orientation	Number of sites	Average site Spacing
L2	347	N42°W	35	9.5 km 4 km in Longmenshan
L1	400	N42°W	38	10 km 4.5 km in Longmenshan
L4	154	N42°W	34	3.7 km

Table DR2. Parameters used in the inversion and r.m.s misfit for each profiles.

Profile	Final r.m.s. misfit	Tau	Error floor				Number of cells in inversion model	
			ρ_{TE}	φ_{TE}	ρ_{TM}	φ_{TM}	Horizontal	Vertical
L2	1.83	100	0.5	0.1	0.1	0.1	164	300
	1.63	30	0.5	0.1	0.1	0.1	164	300
	1.49	10	0.5	0.1	0.1	0.1	164	300

	1.39	3	0.5	0.1	0.1	0.1	164	300
	1.31	1	0.5	0.1	0.1	0.1	164	300
L1	2.058	100	0.5	0.1	0.1	0.1	121	300
	1.82	30	0.5	0.1	0.1	0.1	121	300
	1.68	10	0.5	0.1	0.1	0.1	121	300
	1.57	3	0.5	0.1	0.1	0.1	121	300
	1.49	1	0.5	0.1	0.1	0.1	121	300
L4	2.77	100	0.5	0.1	0.1	0.1	110	300
	2.53	30	0.5	0.1	0.1	0.1	110	300
	2.35	10	0.5	0.1	0.1	0.1	110	300
	2.20	3	0.5	0.1	0.1	0.1	110	300
	2.03	1	0.5	0.1	0.1	0.1	110	300

Table DR3a. Static shift correction factors (fc) for L1

Site number	static correction factor	
	TE Mode	TM Mode
105	0.4	1.0
106	2.8	1.0
107	0.6	1.0
109	1.56	1.0
112	0.15	1.0
116	1.0	7.0
118	0.35	1.0
118a	7.3	1.0
128	3.4	1.0
129	3.6	1.0
134	2.0	1.0

Note: no correction is indicated by fc=1.0

Table DR3b. Static shift correction factors (fc) for L2

Site number	static correction factor	
	TE Mode	TM Mode
201	2.0	1.0
202	1.6	1.0
207	0.6	1.0
208	5.5	1.0
211a	0.35	1.0
213	8.8	1.0
214	0.4	1.0
214a	0.3	1.0
215	0.43	1.0
216	2.68	1.0
217a	7.9	1.0
220	4.12	1.0
223	0.6	1.0
226	0.7	1.0
229	2.0	1.0

Note: no correction is indicated by fc=1.0

Table DR3c. Static shift correction factors (fc) for L4

Site number	static correction factor	
	TE Mode	TM Mode
400	1.0	6.6
401	5.5	1.0
404	0.18	1.0
405	0.06	1.0
406	0.09	1.0
407	3.54	1.0

408	2.13	1.0
410	2.4	1.0
412	4.0	1.0
416	1.0	10
417	1.0	6.5
419	2.8	1.0
421	0.24	1.0
423	0.25	1.0
426	1.0	0.07
436	2.48	1.0
440	0.65	1.0
441	1.82	1.0

Note: no correction is indicated by fc=1.0

Item 8. Supplementary Discussion

Item 8.1) Magnetotelluric (MT) data collection in the Longmenshan

After the Wenchuan earthquake, magnetotelluric (MT) measurements were carried out along three profiles (L2, L1 and L4) that crossed the Longmenshan near the earthquake epicenter during February-May of 2009 (Table DR1 and Figure DR1). Profiles L1 and L2 passed through the most devastated areas and L1 passed directly through the epicenter of the main shock. Additional MT data were collected in October 2009 to increase the station density where rapid changes in crustal resistivity structure were observed. Complementary measurements at some sites in the epicenter region were carried out in 2011. These additional MT measurement have enhanced the MT data quality at some sites, but due to the reconstruction after the Wenchuan earthquake and the rugged topography, the site spacing and data quality at a few sites were still suboptimal in the epicentral area. Seven sets of Phoenix Geophysics V5-2000 broadband MT instruments were used in the field work including one at a permanent remote reference station. Data were recorded in the frequency band 300 -

0.0003 Hz. Five electromagnetic field components were recorded at each site (north-south and east-west electric and magnetic fields and vertical magnetic fields). Robust time series data processing was applied to the data at each site. High quality data at 117 sites on three profiles were selected for subsequent analysis (Table DR1 and Figure DR1).

Item 8.2) Details of 2-D inversions of the magnetotelluric data

Item 8.2.1) Geoelectric strike direction

Analysis using the phase tensor technique (Caldwell et al., 2004; Cai, 2009, in this file) indicates that the skew at most sites is less than 0.2 giving support for a 2D modeling and inversion approach. The geoelectric strike direction is consistently around N45°E for all three profiles. This agrees with the well-defined geological strike direction of the Longmenshan and is perpendicular to the profile orientation as planned (Fig.DR1). Therefore it is reasonable to use 2D inversion of the MT data on each profile. In this frame of reference, the transverse electric (TE) mode comprises the electric field in the direction N45°E and the orthogonal magnetic field. Similarly, the transverse magnetic (TM) mode comprises the electric field in the direction N135°E and the orthogonal magnetic field.

Item 8.2.2) Control parameters

The MT data for each profile were inverted using a conventional 2D inversion algorithm (NLCG) (Rodi et al., 2001, in main text). Topography was included in the inversion. The following control parameters were used in the inversions:

- error floor for TE phase, TM phase and TM apparent resistivity = 10%,
- error floor for TE apparent resistivity = 50%;
- trade-off parameter, $\tau = 10$

Additional details can be found in Table DR2. The first row of the model grid was 10 m in vertical extent and the thickness of subsequent rows increased with depth using a geometric factor in the range 1.2 - 2.0. In the middle crust, where low-resistivity layers were expected, a finer vertical grid interval was used. The size of the grid for

each profile is listed in Table DR2. Inversions started from a uniform halfspace. A wide range of halfspace resistivity values were used for the starting model and all gave essentially the same final resistivity model. The final resistivity models shown in Fig. 2 were obtained using a starting halfspace resistivity of 100 Ωm. The final root-mean-square (r.m.s.) misfits are listed in Table DR2. The fit is also shown in pseudosection format in Figures DR3a,b,c. Note that there is generally good agreement between the measured MT data and the predicted data response. The robustness of the inversion was also investigated using:

(1) different inversion control parameters, such as different error floor and τ,

(2) different starting model,

(3) different sizes of grid etc.

Item 8.2.3) Static shift correction

Static shifts are caused by small-scale, near surface resistivity structures and cause a frequency-independent offset in the apparent resistivity curves. If the static shifts are ignored when the apparent resistivity is used in modeling, the resulting model may contain artifacts (Simpson et al., 2005, in this file). In order to obtain a reliable resistivity model for each MT profile, a static shift correction was made for selected sites on three profiles (Table DR3a, b,c). Static factor fc = 1.0 means no correction was applied. The static coefficients were estimated by the inversion procedure using standard procedures that have been evaluated on field and synthetic data (Unsworth et al., 2005, in main text). Several inversions were performed for each profile with different control parameters for the static shifts. The final static shift coefficients at some sites were chosen based on the data fit at the site and its neighbors. The optimal static shift co-efficients are listed in table DR3a,b,c.

Item 8.3) Interpretation

Before 2008, there was an absence of earthquakes of M=7 or greater in the Longmenshan range, and a 7-year quiet period without events greater than M ≥ 4.

This region is unsual because of the large relief difference (> 4km) across LMS range and thickened crust of the SGb, yet there is a very slow shortening rate (<2mm/yr) as measured by GPS data (Zhang P et al., 2009, in main text).

The emphasis of this paper is to define the resistivity structure of the region and use this to understand the tectonics. The main results of the resistivity model derived by inversion are (1) a high conductivity layer (HCL) in the crust in eastern Tibetan plateau, (2) a high resistivity zone (HRB) beneath Longmenshan Range. Thus each of the three profiles (L1, L2 and L4) was inverted individually using a wide range of inversion parameters. As described in the main text, the inversion models for the three profiles consistently indicate that a HCL occurs at a depth of about 20 km in eastern Tibetan plateau and a HRB is located beneath the Longmenshan. The HRB has nearly the same lateral extent as the "transition zone" (Yu et al., 2010, in main text) and is located in same position as the "rupture unit" (Zhang P et al., 2009, in main text).

The low resistivity pathway connecting the HCL to the surface could be due to the presence of interconnected aqueous fluids. The amount of fluid required can be estimated using Archie's Law. Archie (1942, in this file) proposed an empirical relationship for the bulk resistivity of a fluid saturated rock (ρ) given by

$$\rho = \rho_w \varphi^{-m}$$

where φ is the porosity, ρ_w is the resistivity of the pore fluid and m is the cementation factor. If the fluid is distributed in cracks, then a cementation factor m=1 is applicable corresponding to full connectivity of the fluid phase. From the inversion model for profiles L1, L2 and L4 (Fig.2) the bulk resistivity of the pathway is around 10 -100 Ωm. With a salinity of 5 g/liter, typical of upper crust, this predicts a water resistivity value of ρ_w=1 Ωm (Nesbitt, 1993, in this file) and Archie's Law predicts, a porosity of 1-10% . The lower value reflects m=1 with fluids in cracks and is the most likely scenario. The upper value would be quite unrealistically high. Note that the values listed above are intended as order of magnitude estimates of the fluid content, and reflect the lack of detailed information about crustal fluids in this area.

References cited only in supplementary file

Archie, G. E., 1942, The electrical resistivity log as an aid in determining some reservoir characteristics, *Trans. Am. Inst. Min. Metall. Pet. Eng*., **146**, 54-62.

Cai, J., 2009, The Feature of Three-Dimensional Distortion in magnetotellurics and research of new correction methods: Ph.D. Thesis, Institute of Geology, China Earthquake Administration.

Caldwell, G. T. Bibby, M. H., Brown C., 2004, The magnetotelluric phase tensor: Geophysical Journal International. v.158, p.457 - 469.

Nesbitt, B., 1993, Electrical resistivities of crustal fluids, *J.Geophys. Res.*, **98**, 4301-4310.

Simpson, F. and Bahr, K., 2005, Practical Magnetotellurics: Cambridge University Press. p.111-114.